PAPER

An Extension of Physical Optics Approximation for Dielectric Wedge Diffraction for a TM-Polarized Plane Wave

Duc Minh NGUYEN[†a)], ***Student Member***, **Hiroshi SHIRAI**[†b)], ***Fellow***, ***and*** **Se-Yun KIM**[††c)], ***Nonmember***

SUMMARY In this study, the edge diffraction of a TM-polarized electromagnetic plane wave by two-dimensional dielectric wedges has been analyzed. An asymptotic solution for the radiation field has been derived from equivalent electric and magnetic currents which can be determined by the geometrical optics (GO) rays. This method may be regarded as an extended version of physical optics (PO). The diffracted field has been represented in terms of cotangent functions whose singularity behaviors are closely related to GO shadow boundaries. Numerical calculations are performed to compare the results with those by other reference solutions, such as the hidden rays of diffraction (HRD) and a numerical finite-difference time-domain (FDTD) simulation. Comparisons of the diffraction effect among these results have been made to propose additional lateral waves in the denser media.

key words: *physical optics, PO, edge diffraction, dielectric wedge, uniform asymptotic solution, hidden rays, FDTD, edge condition*

1. Introduction

Among many important problems in wave propagation, edge diffraction by dielectric-edged objects remains a challenging and unsolved diffraction problem. Solutions for this problem play an important role in estimating the scattering of electromagnetic waves by large polygonal obstacles. For a limited number of simple shapes and small objects, the scattering problem can be solved by a number of available exact solutions [1], [2] and numerical methods [3]–[6]. In spite of having reliable accuracy, these methods are not ideal solutions for large objects because they are limited by the time and memory consumption to perform a huge number of calculations. Therefore, developing acceptably fast as well as highly accurate approximation solutions for large objects is truly imperative.

Some high-frequency approximation methods may be able to analyze the scattering field by large conducting objects [7]–[10], such as physical optics (PO) [11]–[16], geometrical theory of diffraction (GTD) [17]–[21], and its extended uniform solutions [22]–[26]. When the scattering objects are made of dielectric materials, the problem becomes more complicated. While the GTD and its extended solutions can be applied only to the conducting objects, a heuristic extension of the uniform theory of diffraction (HUTD) [27] can be used to solve the radiation field in the outer region of the lossy dielectric objects only. This requires us to develop other solutions that can provide a precise evaluation of the scattering field for the inner region of these dielectric objects. For this problem, modified solutions based on the PO method may be possible for edge diffraction in both regions of the penetrable objects. The mathematical foundation for these solutions may be found from the surface equivalence theorem [28]–[30], according to which the scattering fields can be considered as radiation from equivalent electric and magnetic currents on a virtual surface enclosing the scattering body [31]. A uniform asymptotic PO (UAPO) solution has been introduced for the diffraction by dielectric wedges [32], [33]. In this solution, the singularity behaviors at the shadow boundary of the geometrical optics (GO) rays were corrected by using the UTD transition function, in which the non-uniform solution was multiplied by the Fresnel integral. However, the accuracy of the PO for the diffracted field has not been clearly evaluated in this investigation.

The hidden rays of diffraction (HRD) have been proposed to extend a concept of HUTD to the internal diffracted field, in conjunction with the PO currents on the wedge surfaces, and the additionally introduced terms may be interpreted to be excited by the non-physical incident waves [34], [35]. Although the UAPO and HRD approximations are rather simple and powerful tools for estimating the high-frequency diffracted field, their reliability has not been verified clearly yet. This motivates us to evaluate the accuracy of these approximation solutions, and to develop a reliable solution for the edge diffraction by dielectric objects.

In this paper, the diffracted field of a TM-polarized plane wave by a dielectric wedge has been evaluated by an extended PO solution (EPO), in which the radiation fields are obtained by integrating from the equivalent electric and magnetic currents on the wedge surface with two-dimensional Green's function. Unlike conventional PO solutions, these currents are obtained from GO incident, reflected and transmitted rays outside and inside the wedge, respectively. Uniform asymptotic solutions including the error function complement have been derived by using the saddle point technique for scattering field integration. The diffracted fields were then represented in terms of cotangent functions, which have a one-to-one correspondence with the singularities of the shadow boundaries of the GO rays.

Manuscript received July 3, 2023.
Manuscript revised October 2, 2023.
Manuscript publicized November 8, 2023.

[†]The authors are with the Graduate School of Science and Engineering, Chuo University, Tokyo, 112–8551 Japan.
[††]The author is with the Korea Institute of Science and Technology, Seoul, Korea.
a) E-mail: a19.5ekh@g.chuo-u.ac.jp
b) E-mail: shirai@m.ieice.org
c) E-mail: ksy@kist.re.kr

DOI: 10.1587/transele.2023ECP5027

The numerical results were also calculated and compared with those of reference solutions, such as HRD, and the finite-difference time-domain (FDTD) method.

In the following discussion, the time-harmonic factor $e^{j\omega t}$ is assumed and suppressed throughout the text.

2. Derivation of Diffracted Field

When an object is illuminated by an incident electromagnetic wave ($\boldsymbol{E}^{\mathrm{i}}$, $\boldsymbol{H}^{\mathrm{i}}$), the scattered field ($\boldsymbol{E}^{\mathrm{s}}$, $\boldsymbol{H}^{\mathrm{s}}$) may be calculated by the radiation fields from induced electric and magnetic currents on the surface of the object [21], [31]. For the two-dimensional configuration ($\frac{\partial}{\partial z} \equiv 0$), the scattering field ($\boldsymbol{E}^{\mathrm{s}}$, $\boldsymbol{H}^{\mathrm{s}}$) is given by integrating equivalent electric and magnetic currents $\boldsymbol{J}$, $\boldsymbol{M}$ on the boundary C of a scattering body with the Green's function G as [21]

$$\boldsymbol{E}^{\mathrm{s}} = -\int_{\mathrm{C}} \left[j\omega\mu \boldsymbol{J}(\boldsymbol{r}')G(\boldsymbol{r},\boldsymbol{r}') + \boldsymbol{M}(\boldsymbol{r}') \times \nabla' G(\boldsymbol{r},\boldsymbol{r}') \right] dl', \tag{1}$$

$$\boldsymbol{H}^{\mathrm{s}} = -\int_{\mathrm{C}} \left[j\omega\varepsilon \boldsymbol{M}(\boldsymbol{r}')G(\boldsymbol{r},\boldsymbol{r}') - \boldsymbol{J}(\boldsymbol{r}') \times \nabla' G(\boldsymbol{r},\boldsymbol{r}') \right] dl', \tag{2}$$

where a prime denotes the derivative with respect to the source coordinates. Currents $\boldsymbol{J}$ and $\boldsymbol{M}$ are found from the total field ($\boldsymbol{E}$, $\boldsymbol{H}$) on the boundary as

$$\boldsymbol{J} = \hat{\boldsymbol{n}} \times \boldsymbol{H} \qquad \text{on C}, \tag{3}$$

$$\boldsymbol{M} = \boldsymbol{E} \times \hat{\boldsymbol{n}} \qquad \text{on C}, \tag{4}$$

where $\hat{\boldsymbol{n}}$ denotes a unit normal vector on the boundary surface C to the area containing the observation point. While this formulation is mathematically rigorous and the derived field is correct as long as the equivalent currents $\boldsymbol{J}$ and $\boldsymbol{M}$ are precise, the correct current distribution is usually difficult to find. Accordingly, several approximations have been proposed to estimate such currents.

As shown in Fig. 1, let us now consider a two-dimensional dielectric wedge of the wedge angle ϕ_{w} and the relative dielectric constant ε_{r} is illuminated by a TM-polarized incident plane wave:

$$\boldsymbol{H}^{\mathrm{i}} = e^{jkx\cos\phi_0 + jky\sin\phi_0}\hat{\boldsymbol{z}}, \tag{5}$$

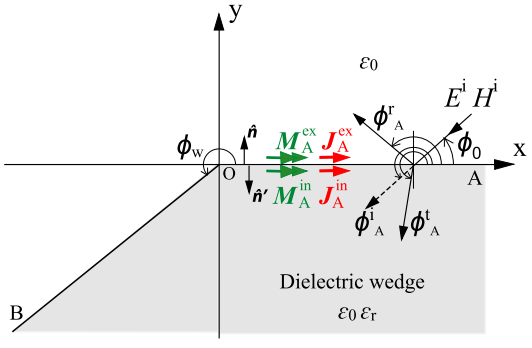

Fig. 1 Plane wave diffraction by a dielectric wedge.

$$\boldsymbol{E}^{\mathrm{i}} = \sqrt{\frac{\mu_0}{\varepsilon_0}} e^{jkx\cos\phi_0 + jky\sin\phi_0} (\sin\phi_0 \hat{\boldsymbol{x}} - \cos\phi_0 \hat{\boldsymbol{y}}), \tag{6}$$

where $k = \omega\sqrt{\varepsilon_0\mu_0}$ denotes the free space wave number, and ϕ_0 is the incident angle.

Depending on the incident direction, the incident wave may illuminate only surface OA ($\phi_0 < \phi_{\mathrm{w}} - \pi$), only surface OB ($\phi_0 > \pi$), or both surfaces ($\phi_{\mathrm{w}} - \pi < \phi_0 < \pi$) of the dielectric wedge. The derivation is illustrated here only for surface OA illumination, and the corresponding result for surface OB illumination is given in Appendix A. In addition, multiple GO reflections may also occur depending on the shape of the wedge and the direction of the incident wave. In order to find a fractional diffraction effect, the wedge angle and the incident angle are somewhat restricted to avoid multiple GO reflections at the wedge surfaces. If these exist, one simply treats these as additional incident waves to derive the corresponding edge diffracted fields.

While our formulation can be extended for lossy dielectric wedges, let us explain here for lossless cases, namely ε_{r} is real positive.

2.1 Exterior Field

The equivalent currents $\boldsymbol{J}$ and $\boldsymbol{M}$ may be approximated from the incident plane wave ($\boldsymbol{E}^{\mathrm{i}}$, $\boldsymbol{H}^{\mathrm{i}}$) in Eqs. (5) and (6) and GO reflected plane wave as

$$\boldsymbol{H}^{\mathrm{r}}_{\mathrm{A}} = \Gamma_A e^{jkx\cos\phi_0 - jky\sin\phi_0}\hat{\boldsymbol{z}}, \tag{7}$$

$$\boldsymbol{E}^{\mathrm{r}}_{\mathrm{A}} = -\Gamma_A \sqrt{\frac{\mu_0}{\varepsilon_0}} e^{jkx\cos\phi_0 - jky\sin\phi_0} (\sin\phi_0 \hat{\boldsymbol{x}} + \cos\phi_0 \hat{\boldsymbol{y}}), \tag{8}$$

with Γ_A is reflection coefficient from surface OA and is given by:

$$\Gamma_{\mathrm{A}} = \frac{\varepsilon_{\mathrm{r}}\sin\phi_0 - \sqrt{\varepsilon_{\mathrm{r}} - \cos^2\phi_0}}{\varepsilon_{\mathrm{r}}\sin\phi_0 + \sqrt{\varepsilon_{\mathrm{r}} - \cos^2\phi_0}}. \tag{9}$$

Then the equivalent currents $\boldsymbol{J}^{\mathrm{ex}}_{\mathrm{A}}$, $\boldsymbol{M}^{\mathrm{ex}}_{\mathrm{A}}$ on surface OA can be approximated as

$$\boldsymbol{J}^{\mathrm{ex}}_{\mathrm{A}} = \hat{\boldsymbol{n}} \times \boldsymbol{H}|_{y=0+} \simeq \boldsymbol{J}^{\mathrm{i}}_{\mathrm{A}} + \boldsymbol{J}^{\mathrm{r}}_{\mathrm{A}} = \hat{\boldsymbol{n}} \times (\boldsymbol{H}^{\mathrm{i}} + \boldsymbol{H}^{\mathrm{r}}_{\mathrm{A}})|_{y=0+}, \tag{10}$$

$$\boldsymbol{M}^{\mathrm{ex}}_{\mathrm{A}} = \boldsymbol{E}|_{y=0+} \times \hat{\boldsymbol{n}} \simeq \boldsymbol{M}^{\mathrm{i}}_{\mathrm{A}} + \boldsymbol{M}^{\mathrm{r}}_{\mathrm{A}} = (\boldsymbol{E}^{\mathrm{i}} + \boldsymbol{E}^{\mathrm{r}}_{\mathrm{A}})|_{y=0+} \times \hat{\boldsymbol{n}}. \tag{11}$$

Substituting $\boldsymbol{J}^{\mathrm{i}}_{\mathrm{A}}$ and $\boldsymbol{M}^{\mathrm{i}}_{\mathrm{A}}$ into Eq. (2), a representative (z) component of the magnetic field H^{iA}_z may be calculated as

$$H^{\mathrm{iA}}_z = \int_0^\infty e^{jkx'\cos\phi_0} \left(-jk\sin\phi_0 G + \frac{\partial G}{\partial y'} \right)_{y'=0} dx', \tag{12}$$

$$G = \frac{-j}{4\pi} \int_{-\infty}^{\infty} \frac{e^{-j\eta(x-x') - j\sqrt{k^2-\eta^2}|y-y'|}}{\sqrt{k^2-\eta^2}} d\eta. \tag{13}$$

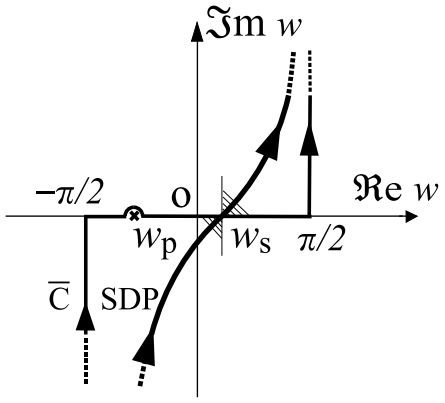

Fig. 2 Integration contours C and SDP in the complex w plane.

Evaluating first the integration with respect to x', one gets

$$H_z^{iA} = \frac{j}{4\pi}\int_{-\infty}^{\infty}\left(\frac{-k\sin\phi_0}{\sqrt{k^2-\eta^2}}\pm 1\right)\frac{e^{-j\eta x - j\sqrt{k^2-\eta^2}|y|}}{(k\cos\phi_0+\eta)}d\eta. \quad (y \gtrless 0) \tag{14}$$

If one uses variable transformation $\eta = k\sin w$, $x = \rho\cos\phi$, $y = \rho\sin\phi$, one gets

$$\begin{aligned} H_z^{iA} &= \frac{j}{4\pi}\int_{\overline{C}}\frac{-\sin\phi_0\pm\cos w}{\cos\phi_0+\sin w}e^{-jk\rho\sin(w\pm\phi)}dw \\ &= \frac{\pm j}{4\pi}\int_{\overline{C}}\cot\frac{\pi/2+w\pm\phi_0}{2}e^{-jk\rho\sin(w\pm\phi)}dw, \quad (\phi \lessgtr \pi) \end{aligned} \tag{15}$$

where the integral contour $\overline{C}$ runs from $(-\pi/2 - j\infty)$ to $(\pi/2 + j\infty)$, as shown in Fig. 2. The above integral may be evaluated by the saddle point technique for $k\rho \gg 1$. Considering the location of the pole $w_p(= \phi_0 - \pi/2)$ and the saddle point $w_s(= |\phi - \pi| - \pi/2)$, one may derive a uniform solution as [2]

$$H_z^{iA} = H_d^{iA} - H_z^{i}U(\phi - \pi - \phi_0), \tag{16}$$

$$H_d^{iA} = -C(k\rho)\left[\cot\frac{\pi-(\phi-\phi_0)}{2} + S^{-}(\phi-\phi_0)U(\pi-\phi)\right], \tag{17}$$

$$C(\chi) = \frac{e^{-j(\chi+\pi/4)}}{\sqrt{8\pi\chi}}, \tag{18}$$

where H_z^{i} represents the z-component of the GO incident plane wave in Eq. (5), and $U(x)$ is a unit step function. A transition function $S^{\pm}(\alpha)$ can be given by

$$\begin{aligned} S^{\pm}(\alpha) = &\frac{1}{\sqrt{\pi}C(k\rho)}e^{jk\rho\cos\alpha}\,\mathrm{sgn}(\pi\pm\alpha) \\ &\cdot Q\left[(1+j)\left|\cos\frac{\alpha}{2}\right|\sqrt{k\rho}\right] - \frac{1}{\cos(\alpha/2)}, \end{aligned} \tag{19}$$

where $Q(y) = \int_y^{\infty} e^{-x^2}dx$ and $\mathrm{sgn}(x)$ is a sign function.

Similarly, one also obtains the magnetic field H_z^{rA} from $\boldsymbol{J}_A^{r}$ and $\boldsymbol{M}_A^{r}$ due to the GO reflected wave as

$$H_z^{rA} = H_d^{rA} + H_{Az}^{r}U(\pi - \phi_0 - \phi), \tag{20}$$

$$H_d^{rA} = -C(k\rho) \cdot \left[\Gamma_A\cot\frac{\pi-(\phi+\phi_0)}{2} + \Gamma_A S^{-}(\phi+\phi_0)U(\pi-\phi)\right], \tag{21}$$

where H_{Az}^{r} represents the z-component of the GO reflected plane wave in Eq. (7).

By combining the contributions from the incident and reflected waves, the exterior diffracted field of the dielectric wedge due to surface OA can be given by:

$$\begin{aligned} H_A^{+} &= H_d^{iA} + H_d^{rA} \\ &= -C(k\rho)\left[\cot\frac{\pi-(\phi-\phi_0)}{2} + S^{-}(\phi-\phi_0)U(\phi-\pi)\right. \\ &\quad \cdot U(\phi_w - \pi - \phi_0) \\ &\quad + \Gamma_A\cot\frac{\pi-(\phi+\phi_0)}{2} + \Gamma_A S^{-}(\phi+\phi_0) \\ &\quad \left.\cdot U(\pi-\phi)U(\pi-\phi_0)\right]. \end{aligned} \tag{22}$$

In the above formulation, the singularity behaviors of cotangent functions match with the shadow boundaries of the GO rays from surface OA. When surface OB is illuminated, the cotangent functions in Eq. (22) are replaced by others corresponding to the incident and reflected waves from surface OB (see Appendix A). The above solution is essentially the same as UAPO [32] but has a different form due to a different treatment near the transition region.

For the perfectly electrically conducting (PEC) wedge, the reflection coefficient Γ_A in Eq. (22) becomes a unit, $\boldsymbol{J}_A = 2\hat{\boldsymbol{n}} \times \boldsymbol{H}^{i}$, and $\boldsymbol{M}_A = 0$. Accordingly, the resulting diffracted field H_A^{+} becomes exactly the same as the one formulated by the PO formulation [16], in which a general formula with four cotangent functions can then be obtained for any incident direction of the PEC wedge problem by combining Eq. (22) and Eq. (A· 1). As mentioned above, these cotangent functions have a one-to-one correspondence with the GO rays. Depending on the direction of the incidence, two GO rays become non-physical rays, and two corresponding cotangent functions cancel out each other to exhibit the correct diffracted field behavior, as reported in [16]. This cancellation occurs even for our uniform expression in Eqs. (22) and (A· 1). On the other hand, when the GO shadow boundary behavior is corrected by multiplying the UTD-type transition function in terms of Fresnel integrals in the UAPO formulation [32], the exact cancellation doesn't occur to yield a small residue to the diffracted field.

2.2 Interior Field

Inside the dielectric wedge, one has only the transmitted

wave ($\boldsymbol{H}_{\mathrm{A}}^{\mathrm{t}}$, $\boldsymbol{E}_{\mathrm{A}}^{\mathrm{t}}$), which can be given by:

$$\boldsymbol{H}_{\mathrm{A}}^{\mathrm{t}} = \mathrm{T}_{\mathrm{A}} e^{-jk_1 x\cos\phi_{\mathrm{A}}^{\mathrm{t}} - jk_1 y\sin\phi_{\mathrm{A}}^{\mathrm{t}}}\hat{\boldsymbol{z}}, \tag{23}$$

$$\boldsymbol{E}_{\mathrm{A}}^{\mathrm{t}} = \mathrm{T}_{\mathrm{A}}\sqrt{\frac{\mu_0}{\varepsilon_{\mathrm{r}}\varepsilon_0}} e^{-jk_1 x\cos\phi_{\mathrm{A}}^{\mathrm{t}} - jk_1 y\sin\phi_{\mathrm{A}}^{\mathrm{t}}}(-\sin\phi_{\mathrm{A}}^{\mathrm{t}}\hat{\boldsymbol{x}} + \cos\phi_{\mathrm{A}}^{\mathrm{t}}\hat{\boldsymbol{y}}), \tag{24}$$

where $k_1 = \omega\sqrt{\varepsilon_{\mathrm{r}}\varepsilon_0\mu_0}$, the transmitted angle $\phi_{\mathrm{A}}^{\mathrm{t}}$ ($\geqslant \pi$) is defined as $\phi_{\mathrm{A}}^{\mathrm{t}} = \pi + \arccos(\cos\phi_0/\sqrt{\varepsilon_{\mathrm{r}}})$, and $\mathrm{T}_{\mathrm{A}} = 1 + \Gamma_{\mathrm{A}}$ is the transmission coefficient from surface OA. Then the corresponding magnetic and electric currents can be obtained as:

$$\boldsymbol{J}_{\mathrm{A}}^{\mathrm{in}} = \hat{\boldsymbol{n}}' \times \boldsymbol{H}_{\mathrm{A}}^{\mathrm{t}}|_{y=0-} = -\mathrm{T}_{\mathrm{A}} e^{-jk_1 x\cos\phi_{\mathrm{A}}^{\mathrm{t}}}\hat{\boldsymbol{x}}, \tag{25}$$

$$\boldsymbol{M}_{\mathrm{A}}^{\mathrm{in}} = \boldsymbol{E}_{\mathrm{A}}^{\mathrm{t}} \times \hat{\boldsymbol{n}}'|_{y=0-} = \mathrm{T}_{\mathrm{A}}\sqrt{\frac{\mu_0}{\varepsilon_{\mathrm{r}}\varepsilon_0}} e^{-jk_1 x\cos\phi_{\mathrm{A}}^{\mathrm{t}}}\sin\phi_{\mathrm{A}}^{\mathrm{t}}\hat{\boldsymbol{z}}. \tag{26}$$

Substituting $\boldsymbol{J}_{\mathrm{A}}^{\mathrm{in}}$ and $\boldsymbol{M}_{\mathrm{A}}^{\mathrm{in}}$ into Eq. (2), the z-component of the internal scattering field due to the transmitted wave on surface OA can be calculated in a similar manner in Eq. (15) as

$$H_{\mathrm{z}}^{\mathrm{tA}} = \frac{-j\mathrm{T}_{\mathrm{A}}}{4\pi}\int_{\overline{\mathrm{C}}} \cot\frac{\phi_{\mathrm{A}}^{\mathrm{t}} - (w - \pi/2)}{2} e^{-jk_1\rho\sin(w-\phi)} dw. \tag{27}$$

Using saddle point technique to evaluate the above integral, $H_{\mathrm{z}}^{\mathrm{tA}}$ can then be written as

$$H_{\mathrm{z}}^{\mathrm{tA}} = H_{\mathrm{A}}^{-} + H_{\mathrm{Az}}^{\mathrm{t}} U(\phi - \phi_{\mathrm{A}}^{\mathrm{t}}), \tag{28}$$

$$H_{\mathrm{A}}^{-} = -C(k_1\rho)\left[\mathrm{T}_{\mathrm{A}}\cot\frac{\phi - \phi_{\mathrm{A}}^{\mathrm{t}}}{2} - \mathrm{T}_{\mathrm{A}} S^{-}(\pi - \phi_{\mathrm{A}}^{\mathrm{t}} + \phi) U(\phi - \phi_{\mathrm{w}}) \cdot U(\pi - \phi_0)\right], \tag{29}$$

where $H_{\mathrm{Az}}^{\mathrm{t}}$ represents the z-component of the GO transmitted plane wave in Eq. (23). The singularity of the cotangent function in Eq. (29) has a one-to-one correspondence with the shadow boundary of the transmitted wave on surface OA. As same as the exterior field, one may have another contribution H_{B}^{-} from the transmitted wave on surface OB as represented by Eq. (A· 2) in Appendix A, as the surface OB is illuminated.

3. Numerical Results and Discussion

In order to evaluate the accuracy of our extended PO (EPO)[†] approximation solution, the numerical results were computed and compared with those obtained from the HRD and FDTD simulation. For convenience, the diffracted field by the HRD solution has been summarized in Appendix B. In order to avoid the multiple internal reflections of the transmitted rays, a rather flat-angle wedge is selected for the numerical example. While the results of EPO are derived from Eqs. (22), (29), (A· 1) and (A· 2), those by HRD can be found from Eqs. (A· 4) and (A· 5) in Appendix B. On the other hand, the diffracted field constituent of FDTD is obtained numerically by subtracting the GO rays from the total field in the following comparisons. The numerical FDTD calculation is rather simple, but the current 2D wedge body spans infinitely. Then one has to select an appropriate transient time to avoid the spurious diffraction effect from the absorbing boundaries. To obtain reliable FDTD simulation results, the following parameters are selected: the frequency is 6 GHz (λ = 50 mm); the analytical region whose center is located at the edge, is 700 mm×700 mm; the rectangular Yee cell size is 0.25 mm × 0.25 mm; and the number of iteration is 50000.

Figure 3 shows the patterns of the total and diffracted fields of a PEC wedge given by the EPO, HRD, and FDTD simulation for a two-side illumination case, in which the EPO has the same result as the conventional PO solution. In this case, the incident wave excites the reflected fields from both surfaces OA and OB. As can be seen from Figs. 3 (a) and 3 (b), the amplitude and the phase of the total field of the three solutions match pretty well in all directions. While the HRD and FDTD results are almost identical, some differences from the EPO result can be observed near the wedge surface. These differences are due to the fact that the diffracted field by the EPO solution doesn't satisfy the boundary and edge conditions [16], [21], [34]. To show the difference more clearly, Fig. 3 (c) is prepared to show the diffracted fields without GO components. The diffracted field is small compared with the GO rays and distributes mainly in the vicinity of the geometrical shadow boundaries SB[r]. As mentioned in Appendix B, the HRD solution is composed from the heuristic UTD diffracted solution of the lossy dielectric wedge [27] to extend for diffracted fields inside the dielectric wedge. Accordingly, the HRD solution coincides exactly with the conventional UTD solution for the PEC wedge [24], and the solution satisfies the boundary and the edge conditions as well. While non-physical parts of the HRD solution contribute to satisfying the boundary condition, the index n relates to the edge condition [36]. One observes a correct behavior of the diffracted field by HRD: the angular derivative (E_ρ) of the diffracted field (H_{z}) becomes zero at the PEC boundary.

When the PEC wedge is replaced by a dielectric wedge of dielectric constant ε_{r} = 6, the corresponding results are shown in Fig. 4. In this case, the incident wave excites the reflected and transmitted waves from both surfaces OA and OB. As can be seen from Figs. 4 (a) and 4 (b), the total field patterns of three solutions also have a good agreement. One observes that the exterior scattering pattern is quite similar to the PEC case in Fig. 3, while the incident wave mostly transmits into the dielectric region to yield a main scattering lobe in the forward direction. Figure 4 (c) shows small differences of diffracted fields among three results. In contrast to the PEC wedge case, it can be seen that the results

[†]As the terminology 'PO' has been often used only for the cases of PEC scattering problems, the word 'extended' is added to show the difference between the conventional PO and our EPO for dielectric problems. EPO reduces to PO for PEC problems.

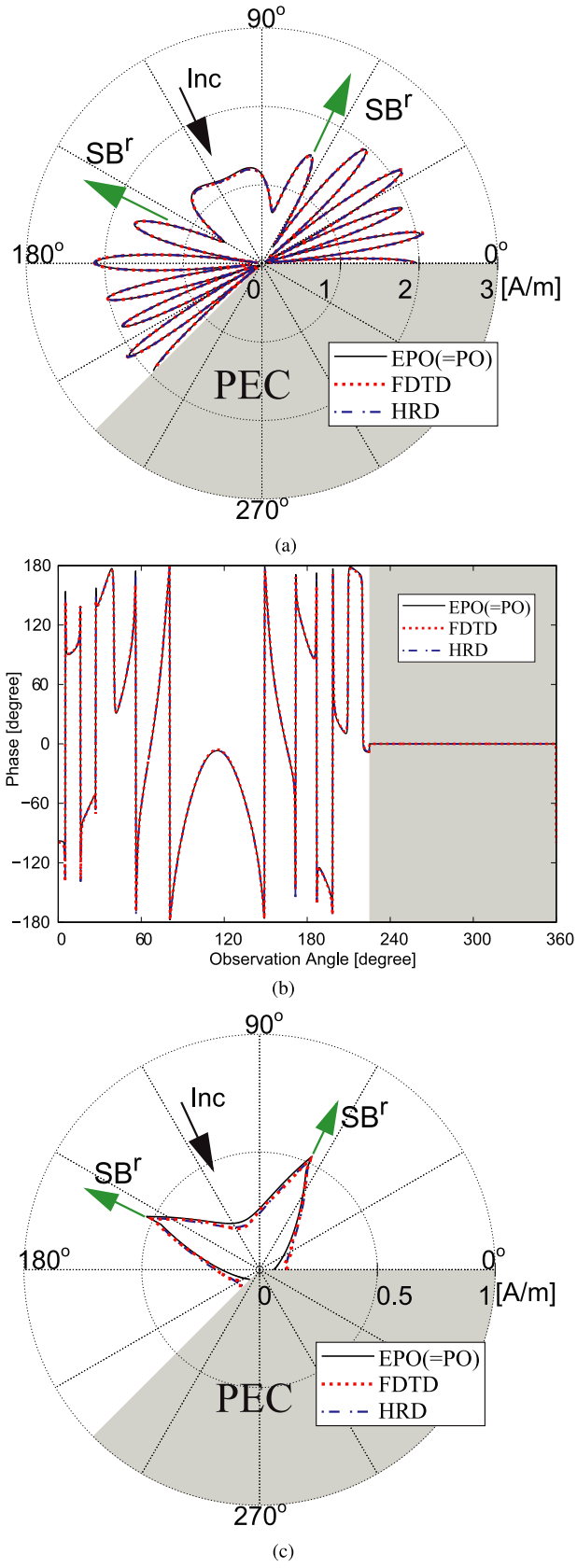

Fig. 3 Total and diffracted fields by PEC wedge: $\phi_w = 225°$, $\phi_0 = 115°$ and $\rho = 3\lambda$. (a) Amplitude of total field. (b) Phase of total field. (c) Amplitude of diffracted field.

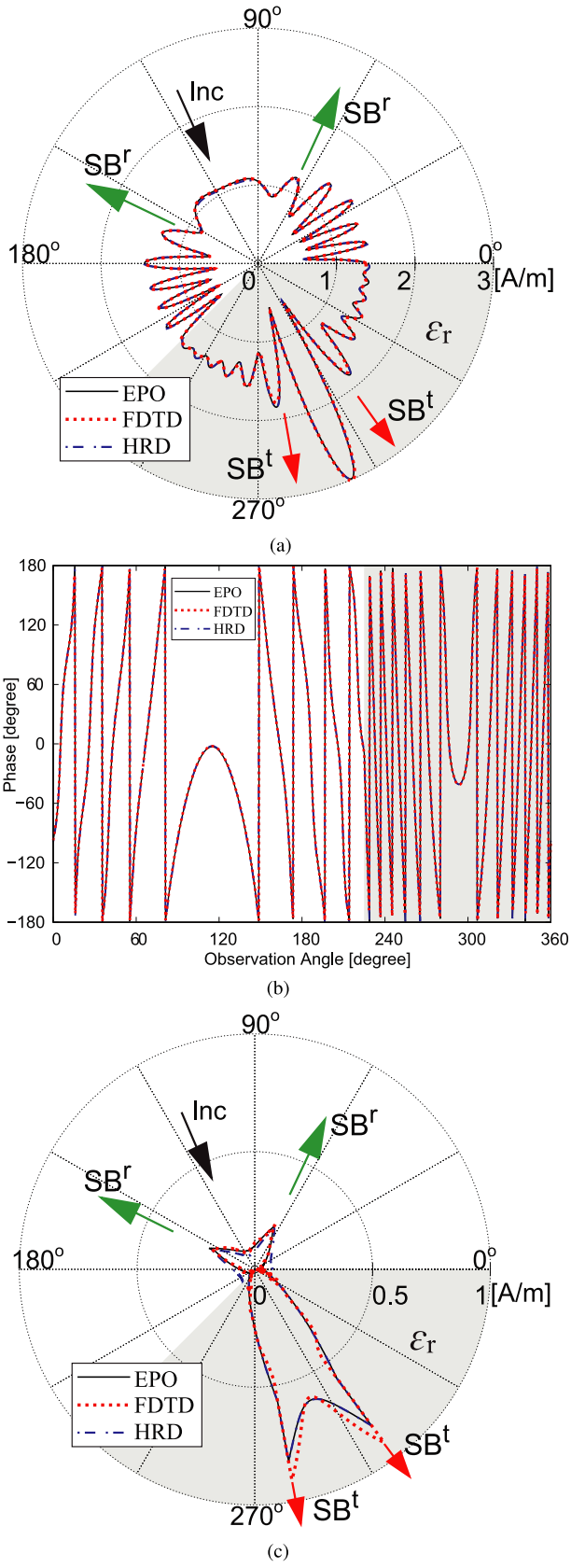

Fig. 4 Total and diffracted fields by dielectric wedge: $\phi_w = 225°$, $\phi_0 = 115°$, $\varepsilon_r = 6$ and $\rho = 3\lambda$. (a) Amplitude of total field. (b) Phase of total field. (c) Amplitude of diffracted field.

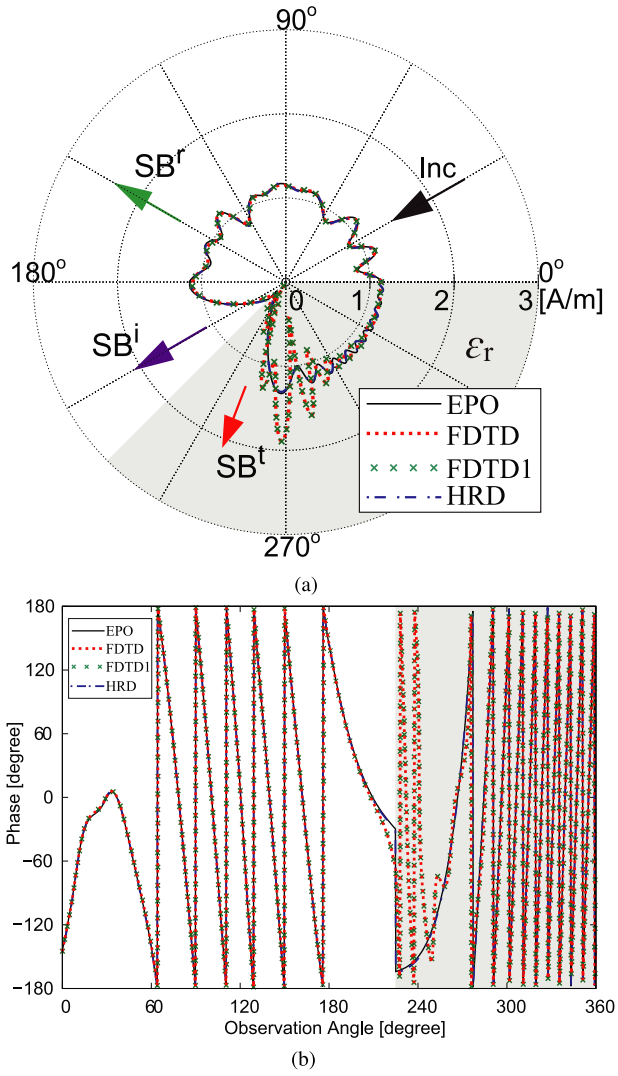

Fig. 5 Total field by dielectric wedge: $\phi_w = 225°$, $\phi_0 = 30°$, $\varepsilon_r = 6$ and $\rho = 3\lambda$. (a) Amplitude of total field. (b) Phase of total field.

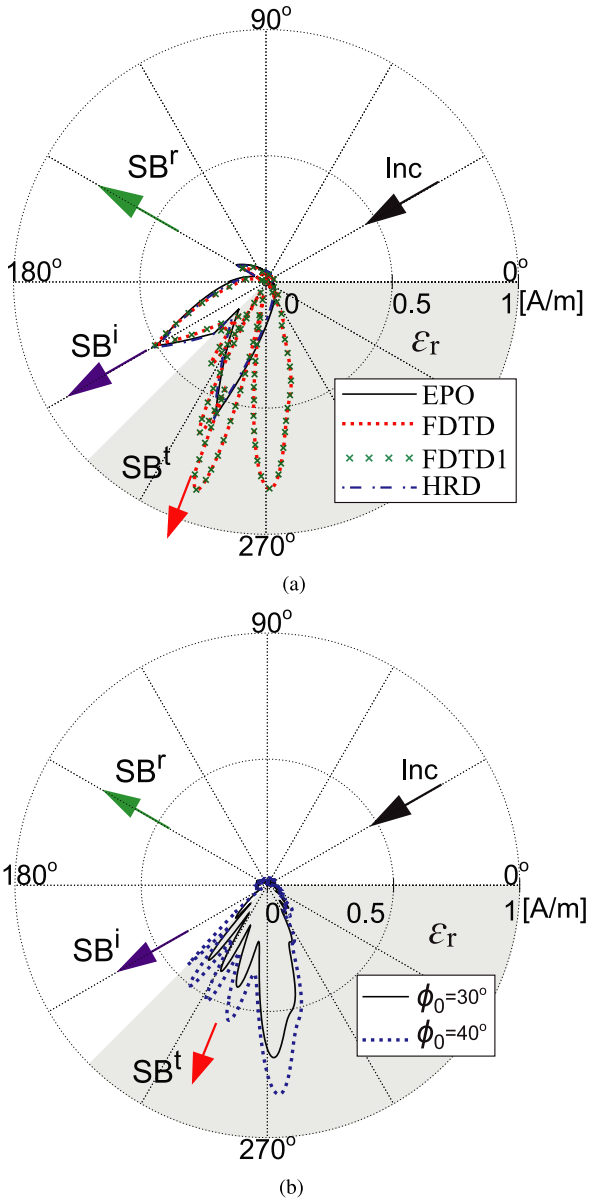

Fig. 6 Amplitudes of diffracted and unexplained remainder fields by dielectric wedge: $\phi_w = 225°$, $\varepsilon_r = 6$ and $\rho = 3\lambda$. (a) Diffracted field for $\phi_0 = 30°$. (b) Unexplained remainder fields for $\phi_0 = 30°$ and 40°.

by EPO match well with the FDTD simulation, while those by HRD show some differences. So far, we cannot explain why the EPO solution becomes better than the HRD solution. This accuracy change of EPO and HRD may be related to the edge condition. For the inside region, the diffracted fields by the EPO and HRD solutions in Fig. 4 (c) exhibit almost the same twin peaks at the transmission shadow boundaries SB^t and have some differences from the FDTD simulation. One observes that, unlike the PEC wedge, both EPO and HRD solutions don't satisfy the boundary condition for the dielectric case. This requires us to consider the missing contributions from the boundary of the dielectric wedge.

When the incident angle ϕ_0 is selected as 30°, only surface OA is illuminated and the corresponding numerical results of the total field are shown in Fig. 5. One observes that all three results match well in the exterior region, while there are some differences in the interior region in Fig. 5 (a). These differences are bigger than those of the two-side illumination case in Fig. 4. An additional calculation (denoted as FDTD1) with cell size of 0.15 mm × 0.15 mm has also been performed to confirm the validity of the previous FDTD calculations. It can be seen that the accuracy of the FDTD results doesn't change even if a significantly smaller cell size is selected. A significant phase change near the wedge surface can be seen for the FDTD result in Fig. 5 (b). This is due to the fact that relatively small FDTD numerical values give erroneous phase, and the analytical EPO and HRD give correct phase change in this range. The difference has been found in the diffracted field in Fig. 6 (a), in which additional field constituent seems to radiate in the interior region. Figure 6 (b) shows the remainder field subtracted our EPO result from the FDTD result in Fig. 6 (a). The corresponding result for $\phi_0 = 40°$ is also plotted in Fig. 6 (b). One observes that

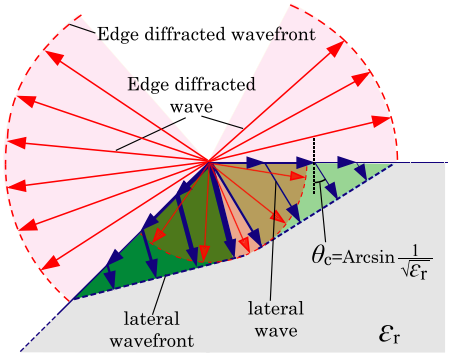

Fig. 7 Possible lateral waves excited by edge diffracted surface waves.

the remainder field becomes larger but has the same shape when the incident angle is selected as 40°.

While the GO contributions satisfy the boundary condition on the wedge surface by the reflection/transmission coefficient, the edge diffracted field excited at the wedge tip doesn't satisfy it. This is due to the fact that the edge diffracted field as in Eq. (22) and Eq. (29) propagates in both outer and inner wedge regions but with different wave numbers. This difference should be compensated by the lateral waves excited in the denser medium. Figure 7 shows an outline sketch of the lateral wave inspired by the radiation field by a line source located at the interface between two media [2]. The excitation of these lateral waves should be dependent on the edge diffracted surface field. One notices from Fig. 6 (a) that the edge diffracted surface field at $\phi = 225°$ is stronger than the one at $\phi = 0°$. Accordingly, the lateral wave is stronger in the vicinity of surface OB. So far, we have not yet found how to augment this lateral wave into our EPO solution.

4. Conclusion

In this paper, the EPO approximation method has been utilized to study the edge diffraction by a dielectric wedge for a TM-polarized plane wave incidence. Here, the scattering field can be formulated by integrating the electric and magnetic currents excited on the illuminated dielectric interface with two-dimensional Green's function. By using the saddle point technique to evaluate the integrations, the uniform asymptotic solutions have been derived.

Comparisons of the numerical results have been made with other reference methods. Good comparisons were observed to confirm the reliability of our EPO for the external field of the dielectric wedge. For the internal field, the EPO and HRD results have been found to exhibit almost the same results. Accordingly, non-physical additional terms introduced by HRD have little effect to the total field, and EPO, which requires significantly fewer computational resources than HRD or FDTD, may be enough to evaluate the edge diffracted field for the dielectric wedge calculation. The difference from the FDTD result suggests an additional diffraction effect, the lateral wave is needed to fill the results by EPO and HRD. The observed change in the accuracy of the EPO and HRD solutions for PEC and dielectric wedges may require careful consideration of the edge condition. These aspects are now under investigation and will be reported in the future.

Acknowledgments

A part of this work has been supported by a Scientific Research Grant In Aide (23K03860, 2023) from the Japan Society for the Promotion of Science, Japan, and 2023 Chuo University Personal Research Grant. The authors thank Profs. T. Uno and T. Arima for their useful advice on the FDTD calculations.

References

[1] J.J. Bowman, T.B.A. Senior, and P.L.E. Uslenghi, Electromagnetic and acoustic scattering by simple shapes, North-Holland, Amsterdam, 1969.
[2] L.B. Felsen and N. Marcuvitz, Radiation and Scattering of Waves, Prentice-Hall, NJ, USA, 1973. (reissued from Wiley-IEEE Press, USA, 1994.)
[3] A. Taflove, Computational Electrodynamics: The Finite-Difference Time-Domain Method, Artech House, Boston, London, 1995.
[4] T. Uno, Electromagnetic Field and Antenna Analysis by FDTD Method, Corona Publ. Co., Japan, 1998 (in Japanese).
[5] R.F. Harrington, Field Computation by Moment Methods, Wiley-IEEE Press, 1993.
[6] P.K. Banerjee and R. Butterfield, Boundary Element Methods in Engineering Science, McGraw-Hill, London, 1981.
[7] J.W. Crispin and K.M. Siegel, Methods of Radar Cross Section Analysis, Academic Press, New York, 1968.
[8] G.T. Ruck, D.E. Barrick, W.P. Stuart, and C.K. Krickbaum, Radar Cross Section Handbook, G.T. Ruck ed., Plenum Press, NY, USA, 1970.
[9] L. Diaz and T. Milligam, Antenna Engineering Using Physical Optics, Artech House, Norwood, MA, USA, 1996.
[10] P. Ya. Ufimtsev, Theory of Edge Diffraction in Electromagnetics, Tech Science Press, Encino, CA, 2003.
[11] M. Ando, "Physical optics," Analysis Methods for Electromagnetic Wave Problems, Chap. 4, E. Yamashita ed., Artech House, Boston, USA, 1990.
[12] S.Y. Kim, J.W. Ra, and S.Y. Shin, "Diffraction by an arbitrary-angled dielectric wedge: Part I – Physical optics approximation," IEEE Trans. Antennas and Propagat., vol.39, no.9, pp.1272–1281, 1991. DOI: 10.1109/8.99035
[13] S.Y. Kim and J.W. Ra, "Diffraction by an arbitrary-angled dielectric wedge: Part II – Correction to physical optics solution," IEEE Trans. Antennas and Propagat., vol.39, no.9, pp.1282–1292, 1991. DOI: 10.1109/8.99036
[14] N.Q. Ta and H. Shirai, "A field equivalence between physical optics and GO-based equivalent current methods for scattering from circular conducting cylinders," IEICE Trans. Electronics, vol.E103-C, no.9, pp.382–387, 2020. DOI: 10.1587/transele.2019ECP5048
[15] N.Q. Ta and H. Shirai, "On the asymptotic evaluation of the physical optics approximation for plane wave scattering by circular conducting cylinders," IEICE Trans. Electronics, vol.E105-C, no.4, pp.128–136, 2022. DOI: 10.1587/transele.2021REP0001
[16] D.M. Nguyen and H. Shirai, "A discussion on physical optics approximation for edge diffraction by a conducting wedge," IEICE Trans. Electronics, vol.E105-C, no.5, pp.176–183, 2022. DOI: 10.1587/transele.2021ECP5031
[17] J.B. Keller, "Diffraction by an aperture," J. Appl. Physics, vol.28, pp.426–444, 1957. DOI: 10.1063/1.1722767

[18] J.B. Keller, "Geometrical theory of diffraction," J. Opt. Soc. Am., vol.52, pp.116–130, Feb. 1962. DOI: 10.1364/JOSA.52.000116
[19] G.L. James, Geometrical Theory of Diffraction for Electromagnetic Waves, Peter Peregrinus Ltd, 1976.
[20] R.C. Hansen, ed., Geometrical Theory of Diffraction, IEEE Press, New York, 1981.
[21] H. Shirai, Geometrical Theory of Diffraction, Corona Publ. Co., Japan, 2015 (in Japanese).
[22] R.M. Lewis and J. Boersma, "Uniform asymptotic theory of edge diffraction," J. Math. Phys., vol.10, pp.2291–2305, 1969. DOI: 10.1063/1.1664835
[23] D.S. Ahluwalia, "Uniform asymptotic theory of diffraction, by the edge of a three dimensional body," SIAM J. Appl. Math., vol.18, pp.287–301, 1970. DOI: 10.1137/0118024
[24] R.G. Kouyoumjian and P.H. Pathak, "A uniform geometrical theory of diffraction for an edge in a perfectly conducting surface," Proc. IEEE, vol.62, pp.1448–1461, 1974. DOI: 10.1109/PROC.1974.9651
[25] S.W. Lee and G.A. Deschamps, "A uniform asymptotic theory of electromagnetic diffraction by a curved wedge," IEEE Trans. Antennas and Propagat., vol.AP-24, pp.25–34, 1976. DOI: 10.1109/TAP.1976.1141283
[26] D.A. McNamara, C.W.I. Pistorious, and J.A.G. Malherbe, Introduction to The Uniform Geometrical Theory of Diffraction, Artech House, 1990.
[27] R.J. Luebbers, "A heuristic UTD slope diffraction coefficient for rough lossy wedges," IEEE Trans. Antennas and Propagat., vol.37, no.2, pp.206–211, 1989. DOI: 10.1109/8.18707
[28] S.A. Schelkunoff, "Some equivalence theorems of electromagnetics and their application to radiation problems," Bell Sys. Tech. J., no.15, pp.92–112, 1936. DOI: 10.1002/j.1538-7305.1936.tb00720.x
[29] R.F. Harrington, Time Harmonic Electromagnetic Fields, McGraw-Hill Co., 1961. (reissued from Wiley-IEEE Press, USA, 2001.)
[30] C.A. Balanis, Advanced Engineering Electromagnetic, 2nd ed., Wiley, NJ, USA, 2012.
[31] H.N. Quang and H. Shirai, "A new interpretation of physical optics approximation from surface equivalence theorem," IEICE Trans. Electronics, vol.E101-C, no.8, pp.664–670, 2018. DOI: 10.1587/transele.E101.C.664
[32] G. Gennarelli and G. Riccio, "A uniform asymptotic solution for the diffraction by a right-angled dielectric wedge," IEEE Trans. Antennas and Propagat., vol.59, no.3, pp.898–903, 2011. DOI: 10.1109/TAP.2010.2103031
[33] M. Frongillo, G. Gennarelli, and G. Riccio, "Plane wave diffraction by arbitrary-angled lossless wedges: high-frequency and time-domain solutions," IEEE Trans. Antennas and Propagat., vol.66, no.12, pp.6646–6653, 2018. DOI: 10.1109/TAP.2018.2876602
[34] S.-Y. Kim, "Hidden rays of diffraction," IEEE Trans. Antennas and Propagat., vol.55, no.3, pp.892–906, 2007. DOI: 10.1109/TAP.2007.891859
[35] S.-Y. Kim, "Hidden rays on the shadow boundaries of penetrable wedges," Proc. 2013 International Symposium on Electromagnetic Theory, pp.778–781, 2013. DOI: 10.34385/proc.30.23PM3F-02
[36] J. Meixner, "The behavior of electromagnetic fields at edges," IEEE Trans. Antennas and Propagat., vol.20, no.4, pp.442–446, 1972. DOI: 10.1109/TAP.1972.1140243

Appendix A: Diffraction Field from Surface OB

When the incident wave illuminates surface OB, equivalent currents $\boldsymbol{J}_{\mathrm{B}}$ and $\boldsymbol{M}_{\mathrm{B}}$ are excited, and the diffracted fields are derived in a similar manner in Sect. 2. The external diffracted field due to $\boldsymbol{J}_{\mathrm{B}}$ and $\boldsymbol{M}_{\mathrm{B}}$ may be given by

$$
\begin{aligned}
H_{\mathrm{B}}^{+} = & -C(k\rho) \\
& \cdot \Bigg[\cot\frac{\pi+(\phi-\phi_0)}{2} + S^{+}(\phi-\phi_0)U(\phi_{\mathrm{w}}-\pi-\phi)U(\phi_0-\pi) \\
& + \Gamma_{\mathrm{B}} \cot\frac{\pi+(\phi+\phi_0-2\phi_{\mathrm{w}})}{2} + \Gamma_{\mathrm{B}} S^{+}(\phi_0+\phi-2\phi_{\mathrm{w}}) \\
& \cdot U(\phi+\pi-\phi_{\mathrm{w}})U(\phi_0+\pi-\phi_{\mathrm{w}}) \Bigg], \qquad (\mathrm{A}\cdot 1)
\end{aligned}
$$

and the internal diffracted field is given by

$$
\begin{aligned}
H_{\mathrm{B}}^{-} = & -C(k_1\rho) \Bigg[-\mathrm{T}_{\mathrm{B}} \cot\frac{\phi-\phi_{\mathrm{B}}^{\mathrm{t}}}{2} - \mathrm{T}_{\mathrm{B}} S^{-}(\pi+\phi_{\mathrm{B}}^{\mathrm{t}}-\phi) \\
& \cdot U(\phi-\phi_{\mathrm{w}})U(\phi_0+\pi-\phi_{\mathrm{w}}) \Bigg], \qquad (\mathrm{A}\cdot 2)
\end{aligned}
$$

where the transmitted angle $\phi_{\mathrm{B}}^{\mathrm{t}}$ is defined as $\phi_{\mathrm{B}}^{\mathrm{t}} = \phi_{\mathrm{w}} + \arccos\left[\cos(\pi+\phi_0-\phi_{\mathrm{w}})/\sqrt{\varepsilon_{\mathrm{r}}}\right]$, and Γ_{B} is the reflection coefficient from surface OB and is given by

$$
\Gamma_{\mathrm{B}} = \frac{\varepsilon_{\mathrm{r}}\sin(\pi+\phi_0-\phi_{\mathrm{w}}) - \sqrt{\varepsilon_{\mathrm{r}}-\cos^2(\pi+\phi_0-\phi_{\mathrm{w}})}}{\varepsilon_{\mathrm{r}}\sin(\pi+\phi_0-\phi_{\mathrm{w}}) + \sqrt{\varepsilon_{\mathrm{r}}-\cos^2(\pi+\phi_0-\phi_{\mathrm{w}})}}, \qquad (\mathrm{A}\cdot 3)
$$

and $\mathrm{T}_{\mathrm{B}} = 1 + \Gamma_{\mathrm{B}}$.

Appendix B: Hidden Rays of Diffraction (HRD) Solution

One knows that the PO solution does not satisfy the boundary and edge conditions. A concept of hidden rays in the non-physical domain has then been introduced to correct the error of PO [34], [35]. The HRD solution is extended from the HUTD solution and satisfies the boundary and edge conditions for the case of the PEC wedge. The external and internal diffracted fields by a two-dimensional dielectric wedge can be given by the HRD solution, respectively as [34]

$$
\begin{aligned}
\bar{H}^{+} = & -C(k\rho) \\
& \cdot \Bigg[\frac{1}{n}\cot\frac{\pi-(\phi-\phi_0)}{2n} + S^{-}(\phi-\phi_0)U(\phi-\pi) \\
& + \frac{1}{n}\cot\frac{\pi+(\phi-\phi_0)}{2n} + S^{+}(\phi-\phi_0)U(\phi_{\mathrm{w}}-\pi-\phi) \\
& + \frac{\bar{\Gamma}_{\mathrm{A}}}{n}\cot\frac{\pi-(\phi+\phi_0)}{2n} + \bar{\Gamma}_{\mathrm{A}} S^{-}(\phi+\phi_0)U(\pi-\phi) \\
& + \frac{\bar{\Gamma}_{\mathrm{B}}}{n}\cot\frac{\pi+(\phi+\phi_0-2\phi_{\mathrm{w}})}{2n} + \bar{\Gamma}_{\mathrm{B}} S^{+}(\phi_0+\phi-2\phi_{\mathrm{w}}) \\
& \cdot U(\phi+\pi-\phi_{\mathrm{w}}) \Bigg], \qquad (\mathrm{A}\cdot 4)
\end{aligned}
$$

$$
\begin{aligned}
\bar{H}^{-} = & -C(k_1\rho) \\
& \cdot \Bigg[\frac{\bar{\mathrm{T}}_{\mathrm{A}}}{n}\cot\frac{\phi-\phi_{\mathrm{A}}^{\mathrm{t}}}{2n} - \bar{\mathrm{T}}_{\mathrm{A}} S^{-}(\pi-\phi_{\mathrm{A}}^{\mathrm{t}}+\phi)U(\phi-\phi_{\mathrm{w}})
\end{aligned}
$$

$$-\frac{\bar{\mathrm{T}}_\mathrm{B}}{n}\cot\frac{\phi-\phi_\mathrm{B}^\mathrm{t}}{2n}-\bar{\mathrm{T}}_\mathrm{B}S^{-}(\pi+\phi_\mathrm{B}^\mathrm{t}-\phi)U(\phi-\phi_\mathrm{w})\Bigg], \tag{A·5}$$

where $\bar{\Gamma}_\mathrm{A}$ and $\bar{\Gamma}_\mathrm{B}$ are the reflection coefficients of surfaces OA and OB, and given by

$$\bar{\Gamma}_\mathrm{A}=\frac{\varepsilon_\mathrm{r}|\sin\phi_0|-\sqrt{\varepsilon_\mathrm{r}-\cos^2\phi_0}}{\varepsilon_\mathrm{r}|\sin\phi_0|+\sqrt{\varepsilon_\mathrm{r}-\cos^2\phi_0}} \tag{A·6}$$

$$\bar{\Gamma}_\mathrm{B}=\frac{\varepsilon_\mathrm{r}|\sin(\pi+\phi_0-\phi_\mathrm{w})|-\sqrt{\varepsilon_\mathrm{r}-\cos^2(\pi+\phi_0-\phi_\mathrm{w})}}{\varepsilon_\mathrm{r}|\sin(\pi+\phi_0-\phi_\mathrm{w})|+\sqrt{\varepsilon_\mathrm{r}-\cos^2(\pi+\phi_0-\phi_\mathrm{w})}}. \tag{A·7}$$

$\bar{\mathrm{T}}_\mathrm{A}=1+\bar{\Gamma}_\mathrm{A}$ and $\bar{\mathrm{T}}_\mathrm{B}=1+\bar{\Gamma}_\mathrm{B}$ are corresponding transmission coefficients of surfaces OA and OB, respectively. The index parameter n is taken by the minimum positive value satisfying the edge condition as [34]

$$\tan\frac{2\pi-\phi_\mathrm{w}}{n}=\varepsilon_\mathrm{r}\tan\frac{-\phi_\mathrm{w}}{n}. \tag{A·8}$$

The HRD formulations in Eqs. (A·4) and (A·5) may be applied to any direction of the incident wave, while one may need additional multiple diffracted field contributions due to particular incident and wedge angles.

Duc Minh Nguyen received the B.E. in Telecommunication Engineering from Hanoi University of Science and Technology, and the M.E. degree in Electrical, Electronic, and Communication Engineering from Chuo University, Japan, in 2018 and 2021, respectively. He is now a Ph.D. student at Chuo University. His current research interest is electromagnetic scattering. Mr. Nguyen is a student member of the IEEE.

Hiroshi Shirai received the B.E. and the M.E. degrees in Electrical Engineering from Shizuoka University, Japan, in 1980 and 1982, respectively, and the Ph.D. degree from Polytechnic University (presently renamed as Tandon School of Engineering, New York University), New York in 1986. He was a Research Fellow, then a Postdoctoral Scientist until March 1987 at Polytechnic University. Since April 1987, he has been with Chuo University, Tokyo, Japan, where he is currently a Vice President, Director of International Center and a Professor. He has been serving as a committee member of various technical societies and international meetings. He is now an Editorial Advisory member of IEICE Fundamentals Review. He received the R.W.P. King Best Paper Award from the Antennas and Propagation Society of the IEEE in 1987, the IEICE Electronics Society Award in 2019, and the IEICE Best Paper Award in 2020. His current research interests include wave propagation and diffraction in time-harmonic and transient domains. Dr. Shirai is a Fellow of the Electromagnetic Academy, a senior member of the IEEE, a member of Sigma Xi, and the IEE of Japan.

Se-Yun Kim received the B.S. degree from Seoul National University, Seoul, Korea in 1978 and the M.S. and Ph.D. degrees from the Korea Advanced Institute of Science and Technology, Seoul, Korea in 1980 and 1984, respectively, all in electrical engineering. He was a Postdoctoral Fellow from 1984 to 1986 at the Korea Advanced Institute of Science and Technology. In 1986, he joined the Korea Institute of Science and Technology, Seoul, Korea, where he retired formally in 2020 and is now an Honorary Researcher. His research interests include electromagnetic diffraction, microwave imaging, and geophysical probing. Dr. Kim received the Academic Achievement Award from the Institute of Electronics and Information Engineers in 1988, the Order of National Security Merit from the Korean Government in 1990, and the Paper Award at the ISAP 2007, Niigata, Japan. He has been the Man of National Merit since 1991.